

Article

Studied Localized Surface Plasmon Resonance Effects of Au Nanoparticles on TiO₂ by FDTD Simulations

Guo-Ying Yao, Qing-Lu Liu and Zong-Yan Zhao *

Faculty of Materials Science and Engineering, Kunming University of Science and Technology, Kunming 650093, China; ygy0046@163.com (G.-Y.Y.); qluliu@kmust.edu.cn (Q.-L.L.)

* Correspondence: zzy@kmust.edu.cn; Tel.: +86-871-65109952; Fax: +86-871-65107922

Received: 7 April 2018; Accepted: 21 May 2018; Published: 5 June 2018



Abstract: Localized surface plasmon resonance (LSPR) plays a significant role in the fields of photocatalysis and solar cells. It can not only broaden the spectral response range of materials, but also improve the separation probability of photo-generated electron-hole pairs through local field enhancement or hot electron injection. In this article, the LSPR effects of Au/TiO₂ composite photocatalyst, with different sizes and shapes, have been simulated by the finite difference time domain (FDTD) method. The variation tendency of the resonance-absorption peaks and the intensity of enhanced local enhanced electric field were systematically compared and emphasized. When the location of Au nanosphere is gradually immersed into the TiO₂ substrate, the local enhanced electric field of the boundary is gradually enhanced. When Au nanospheres are covered by TiO₂ at 100 nm depths, the local enhanced electric field intensities reach the maximum value. However, when Au nanorods are loaded on the surface of the TiO₂ substrate, the intensity of the corresponding enhanced local enhanced electric field is the maximum. Au nanospheres produce two strong absorption peaks in the visible light region, which are induced by the LSPR effect and interband transitions between Au nanoparticles and the TiO₂ substrate. For the LSPR resonance-absorption peaks, the corresponding position is red-shifted by about 100 nm, as the location of Au nanospheres are gradually immersed into the TiO₂ substrate. On the other hand, the size change of the Au nanorods do not lead to a similar variation of the LSPR resonance-absorption peaks, except to change the length-diameter ratio. Meanwhile, the LSPR effects are obviously interfered with by the interband transitions between the Au nanorods and TiO₂ substrate. At the end of this article, three photo-generated carrier separation mechanisms are proposed. Among them, the existence of direct electron transfer between Au nanoparticles and the TiO₂ substrate leads to the enhanced local enhanced electric field at the boundaries, which is favorable for the improvement of photocatalytic performance of TiO₂. These findings could explain the underlying mechanism of some experimental observations in published experimental works, and helpful to design highly efficient composite photocatalysts that contain noble metal co-catalyst nanoparticles.

Keywords: photocatalysis; localized surface plasmon resonance; Au nanoparticle; FDTD simulation

1. Introduction

TiO₂ is a kind of fascinating photocatalyst that possesses the ability of splitting water, which was first observed by Fujishima and Honda [1]. Afterwards, many scientists have also made many contributions in photocatalytic technology, such as clarifying the intrinsic mechanism, improving the photocatalytic performance, and exploring novel efficient photocatalysts. It is well known that TiO₂ can only be activated by UV-light irradiation, whose energy accounts for only 5% of the solar spectrum. In order to make efficient use of solar energy, researchers have performed a large number of studies to improve the photocatalytic performance of TiO₂. The most conventional strategy is

doping with metals [2,3] or non-metals [4,5] into the TiO₂ lattice. This approach can narrow the band gap of TiO₂ to absorb visible light. However, as the impurities are introduced, it inevitably has some intrinsic shortcomings, and the effects of the modification are very limited. Meanwhile, using a noble metal as a co-catalyst loaded onto the surface of TiO₂ is another effective modification strategy to choose [6,7]. The co-catalyst is used as an electron trap to suppress the recombination of photo-generated electron-hole pairs, resulting in the improvement of photocatalytic performance.

The optical properties of metal nanoparticles are known to be characterized primarily by the collective vibration of their free electrons, the so-called localized surface plasmon resonance (LSPR). Initially, LSPR plays an important role in biosensors, which have a very high sensitivity in the detection of biomolecular-specific interaction analysis. Until 2008, Awazu et al. placed the LSPR effects in the field of photocatalysis and presented the concept of plasmonic photocatalysis [8], which attracted more researchers to focus on this subject. For example, Tanaka et al. prepared spherical gold particles supported on TiO₂, which exhibited excellent performance due to LSPR, and the apparent quantum efficiency reached 7.2% in the visible-light region [9]. LSPR can directly extend the light absorption range of TiO₂ to the visible region without reducing the band gap value of TiO₂, which is different with the doping modification method. For example, Feng et al. have found a new strong absorption peak at 560 nm in the case of Cu/TiO₂ composite photocatalyst under the visible-light region [10]; Mubeen et al. also observed that the absorption spectrum of Au/TiO₂ composite photocatalyst extends to 620 nm [11].

It is known that metal nanoparticles, such as gold (Au) [12–14], silver (Ag) [15–17], copper (Cu) [18–20], and bismuth (Bi) [21], also show strong optical absorption due to LSPR in the visible-light region. Among them, Au has attracted extensive concern, due to its excellent catalytic performance and remarkable LSPR effects. Thus, it has been used as a catalyst/co-catalyst in many composite photocatalysts, such as Au/Cu₂O [12,22], Au/TiO₂/g-C₃N₄ [23], and Au/La₂Ti₂O₇ [24]. In these cases, the photocatalytic performance is significantly promoted because Au particles not only act as electron traps and active sites, but also induce the LSPR effects. According to the generation mechanism of LSPR, the size, shape, and composition of metallic nanoparticles are the key factors that predominately determined the effects of LSPR. Therefore, many research groups have focused on how to regulate and utilize the LSPR effect through the selection of materials and the design of micro/nano-structures. On the other hand, the optical properties of metallic nanoparticles are also determined by the electron interband transition with the substrate. However, energetic charge carriers created by the Au interband transitions are frequently ignored in the field of photocatalysis. In the present work, Au nanoparticles supported on a TiO₂ substrate are chosen as the research subject. Herein, we report the change of the size and shape of Au nanoparticles loaded on the different positions of the TiO₂ substrate. Furthermore, based on finite difference time domain (FDTD) simulated results, the electron interband transition between Au nanoparticles and the TiO₂ substrate are determined, and the potential influences on LSPR effects are also discussed.

2. Results and Discussions

2.1. Au Nanospheres

In the present work, we considered four different locations of Au nanoparticle loading on the TiO₂ substrate as shown in Figure 1: (a) the Au nanoparticle just contacts the surface of the TiO₂ substrate, which is labeled as “Model A”; (b) the Au nanoparticle is half-embedded into the TiO₂ substrate, and the center of the Au nanoparticle coincides with the surface of the TiO₂ substrate, which is labeled as “Model B”; (c) the Au nanoparticle is completely embedded in the TiO₂ substrate, which is labeled as “Model C”; and (d) the Au nanoparticle is embedded in the TiO₂ substrate to a depth of 100 nm beneath the surface, which is labeled as “Model D”. In these models, the configurations of Model C and Model D are similar to the core-shell structure of Au/TiO₂ composite photocatalysts in published experimental work, so they can better model this special nano-structure.

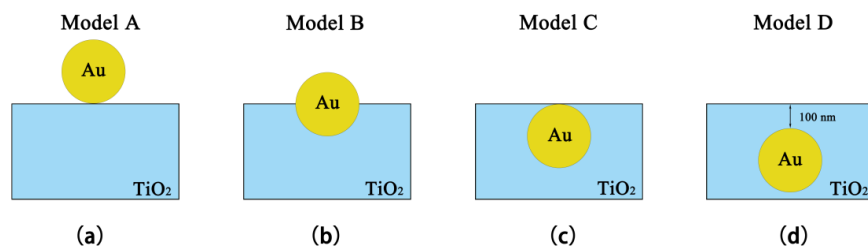


Figure 1. The location of Au nanoparticles loaded on the TiO_2 substrate: (a) The Au nanoparticle just in contact with the surface of the TiO_2 substrate; (b) the Au nanoparticle is half-embedded into the TiO_2 substrate, and the center of the Au nanoparticle coincides with the surface of the TiO_2 substrate; (c) the Au nanoparticle is completely embedded in the TiO_2 substrate; and (d) the Au nanoparticle is embedded in the TiO_2 substrate to a depth of 100 nm beneath the surface.

Due to the high spherical symmetry of Au nanospheres, the plasma oscillations are isotropic, and only exhibit a single LSPR absorption peak in the wavelength range of 300–900 nm, as shown in Figure 2. For isolated Au nanospheres with different radii, their corresponding resonance absorption peaks are centered at different positions in the extinction spectra: 517 nm (for $R = 25$ nm), 530 nm (for $R = 50$ nm), 581 nm (for $R = 75$ nm), and 610 nm (for $R = 100$ nm), respectively. Table 1 shows the corresponding electric near-field intensity at these resonance peaks for different radii of Au nanospheres. It is obviously observed that these peaks are red-shifted with the increase of the radius of the Au nanospheres, which is in accordance with published results [13,25,26]. Furthermore, as the radius of Au nanospheres increases, the extinction coefficient also increases. In the case of Au nanospheres with radii of 25 nm, the extinction coefficient is the smallest (the black curve in Figure 2), which is almost equal to zero, while the corresponding electric near-field intensity reaches the maximum with the Au nanospheres with radii of 75 nm. These simulated results suggest that the features of resonance absorption of LSPR can be tuned by varying the radius of the Au nanospheres.

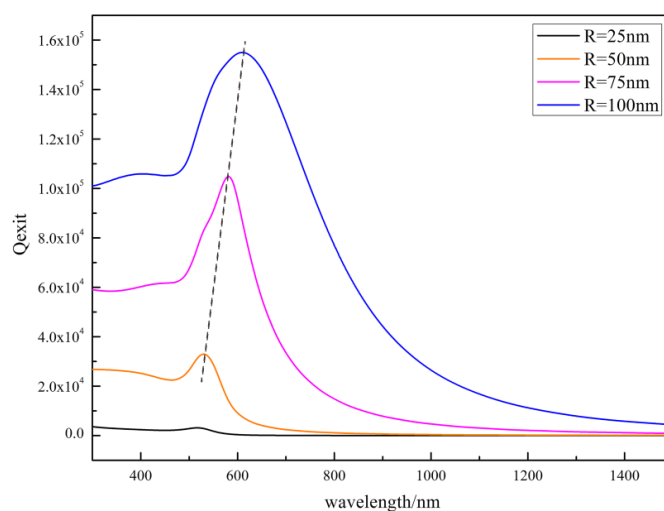


Figure 2. The extinction spectra of isolated Au nanospheres with different radii.

Table 1. The electric near-field intensity of gold nanospheres.

Radius/nm	The Absorption Peak of LSPR/nm	E^2
25	517	4.400
50	530	5.983
75	581	6.412
100	610	4.883

The absorption spectra of Au nanospheres loaded on the TiO₂ substrate at different locations are illustrated in Figure 3. The absorption spectrum of anatase TiO₂ (the green curve) perfectly reproduces those results of experimental measurements [1], implying the calculation method and setting parameters are reliable. In the case of Au nanospheres with radii of 100 nm, there are four absorption peaks that are respectively centered at ~350, ~420, ~520, and ~610 nm in Figure 3a for “Model A”. The absorption peak centered at ~350 nm is undoubtedly produced by the TiO₂ substrate, which is labeled as “a” in Figure 3a. This further shows that there is a strong interaction between Au and TiO₂. This interaction is mainly determined by the interfacial electronic states, resulting in the electron transition from the high occupied states of Au nanoparticles to the valence band of the TiO₂ substrate [27]. Thus, the absorption peak centered at ~420 nm is ascribed to the electronic transitions between Au nanospheres and the TiO₂ substrate, which is labeled as “b” in Figure 3a. As per published experimental measurements, the absorption peak centered at ~520 nm is induced by the LSPR effects, which is labeled as “c” in Figure 3a. There is another shoulder absorption peak centered at ~610 nm, which is labeled as “d” in Figure 3a. For nanoparticles, the electronic energy levels are not continuous, compared to bulk materials, but discrete due to the quantum size effects of the nanoparticles and this can result in a sharp and an intense absorption features corresponding to interband transitions in nanoparticles [28]. According to Guerrisi’s conclusion and Liu’s experiment the absorption edge in Au particles is located at ~1.94 eV (~640 nm), which is produced by the interband electronic transition [29,30]. Thus, it can be speculated that this absorption peak is ascribed to the interband transition in Au nanospheres. When the radius of Au nanospheres decreased from 100 to 25 nm, these four absorption peaks show different trends: (1) the absorption properties produced by the TiO₂ substrate do not present any obvious variation; (2) the absorption peak led by the electronic transition between Au nanospheres and the TiO₂ substrate are gradually blue-shifted and, finally, integrated into the absorption of TiO₂ substrate, which is possibly led by the quantum size effects of the Au nanospheres; (3) the LSPR absorption peak of the Au nanospheres is gradually blue-shifted and decreasing, which is also possibly led by the quantum size effects; (4) the absorption peaks produced by the interband transition of Au nanospheres is gradually red-shifted and decreasing, indicating that the optical absorption of Au nanosphere is severely affected by the interaction between LSPR and local interband transitions [31]. Additionally, in the case of Au nanospheres with radii of 25 nm, the variation of optical absorption properties induced by Au nanosphere loading are insignificant, implying that small Au nanospheres do not respond to the incident light. The above characteristics are presented in Au nanospheres with different particle radii, but there are some differences in the details. For example, the absorption peaks “c” and “d” will be split into several distinct peaks, and vary with respect to the blue-shifting as the sphere radius decreases. This simulated result indicates that LSPR and interband transition will induce multi-peak absorption characteristics, especially in case of Au nanospheres that are completely embedded into the TiO₂ substrate. It has been experimentally demonstrated that the position of plasmon resonance absorption is sensitively dependent on the particle size and progressively shifts to the longer wavelengths with the increase of the particle size [12,32].

When Au nanospheres are gradually embedded into the TiO₂ substrate, the optical absorption properties present some obvious or not obvious variations, as shown in Figure 3 (1) the absorption produced by the TiO₂ substrate maintains the constant characteristics, which means the optical properties of TiO₂ substrate are not impacted by the size and location of Au nanosphere loading; (2) the absorption intensity led by the electronic transition between Au nanospheres and the TiO₂ substrate are gradually decreasing. It can be understood that the interaction between Au nanospheres and TiO₂ substrate is gradually weakened with the loading location immersing; (3) the resonance absorption peak is firstly decreasing and then increasing, and split into several distinct peaks; and (4) the absorption induced by the interband transition is gradually increasing, split into several distinct peaks. These simulated results clearly demonstrate that the LSPR effects are also sensitively dependent on the location of Au nanospheres in the TiO₂ substrate. In addition, it can be clearly observed that the absorption peak of LSPR is red-shifted, as Au nanospheres are gradually immersed in

the TiO₂ substrate. These red-shifts arose due to an overall increase in the refractive index of the dielectric environment surrounding the Au nanospheres upon TiO₂ coating. The core-shell Au-TiO₂ nanostructures, with TiO₂ shells of a high refractive index (2.5) on all sides of the gold cores, experienced a larger red-shift, compared with Model A and B, in which TiO₂ was coated only on one side of the gold, leaving the other side exposed to air, which had a lower refractive index of ≈ 1.4 .

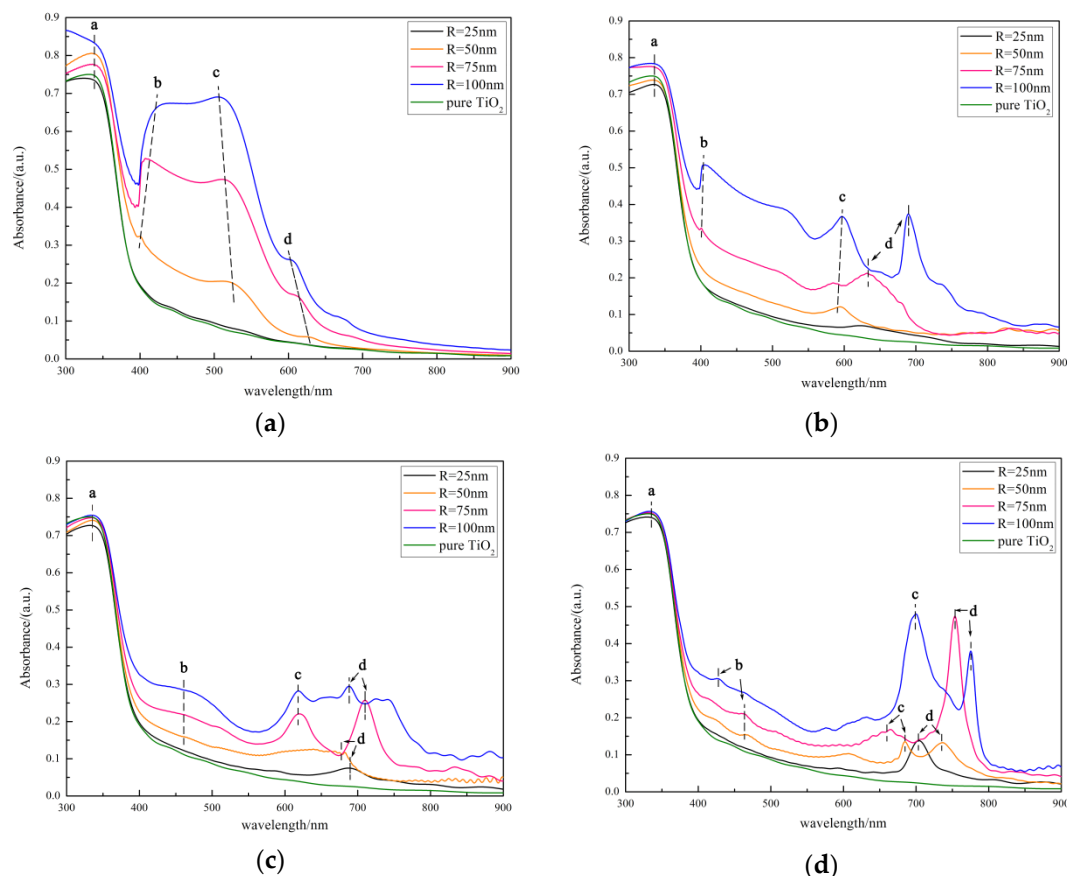


Figure 3. The absorption spectra of Au nanospheres loaded on the TiO₂ substrate with different radii and locations: (a) Model A; (b) Model B; (c) Model C; and (d) Model D as labeled in Figure 1.

In FDTD simulations, the plane-wave source is incident on an Au nanosphere, and the induced electric fields at the particular wavelength around Au nanospheres can be further obtained. In order to further demonstrate the roles of the LSPR effects, the electric field distribution of Au/TiO₂ composite systems for the corresponding absorption peaks of LSPR and interband transitions (“c” and “d”) are respectively illustrated in Figure 4. Subgraph (a) corresponds with the electric field distribution induced by LSPR, and subgraph (b) corresponds with that induced by the interband transitions. Their orders are arranged by the sphere radius and the location of the Au nanosphere. These patterns show the local enhanced electric field is enhanced around Au nanospheres. With the increase in the radius of the Au nanospheres, both enhanced electric fields are gradually increasing. The results show that larger Au nanospheres exhibit more obvious effects on the enhanced electric fields. Therefore, in order to avoid the interference of interband transitions with LSPR, it is experimentally attempted to prepare Au nanospheres with suitable radii. It can be clearly observed that the electric field intensity of the interband transitions is greater than that of LSPR by the electric field diagram of the large-sized gold nanoparticles. Furthermore, it has been reported that the interband transitions of Au correspond to the contribution of Au 5d electrons to the electronic structure of Au [33,34]. Under the excitation of light, the 5d band of gold may generate a large number of electronic transitions and show a strong

electric field. Through LSPR related decay through interband transitions, both LSPR and interband transitions are favorable for light absorption and enhanced the local electric field. When the location of the Au nanospheres is changing, the enhanced electric fields present different variations: both enhanced electric fields firstly decrease, and then increase, as the location of Au nanospheres is gradually embedded into the TiO₂ substrate. In the case of LSPR, when Au nanospheres are completely embedded into the TiO₂ substrate (i.e., Model C), the enhanced electric field is the smallest, as shown in Figure 4a. Especially in the cases of $R = 25$ and 50 nm, the enhanced electric field is equal to zero; in the other words, the electric field is not enhanced by the LSPR effects, while a similar phenomenon could be observed when the Au nanospheres is half embedded into the TiO₂ substrate (i.e., Model B), as shown in Figure 4b.

In the field of photocatalysis, the presence of the local enhanced electric field can effectively separate photo-generated electron-hole pairs. Therefore, except the above discussions for the local enhanced electric fields enhanced by LSPR or the interband transition, the distribution of the strongest local enhanced electric field in the whole simulation region of 300–900 nm are provided in Figure 5, in which the corresponding wavelength is also indicated. It can be determined that Au nanoparticles have strong interaction with the TiO₂ substrate through the strong metal-support interaction compared to the single Au nanoparticle by comparing the electric field intensity of a single Au nanoparticle (Table 1) with the electric field intensity of the Au/TiO₂ composite structure (Figure 5). In the case of Au nanospheres loaded onto the TiO₂ substrate (i.e., Model A), as the radius of the Au nanospheres increases, the local enhanced electric field also gradually increases, and only appears at the interface of the Au nanospheres and the TiO₂ substrate. In the other cases of Models B–D, the phenomenon is just the opposite: the local enhanced electric field gradually decreases as the radius of the Au nanospheres increases. These simulated results suggest that the interface between Au nanospheres and the TiO₂ substrate is the key factor to determine the local enhanced electric field [12,19]. From the combined above discussions and the corresponding wavelength of the strongest local enhanced electric field, it can be concluded that the strongest local enhanced electric field is caused by the interband transition in the case of Model A, and it is more obvious in the larger Au nanospheres, while the strongest local enhanced electric field is caused by LSPR in the cases of Model B, C, and D, and it is more obvious in the smaller Au nanospheres.

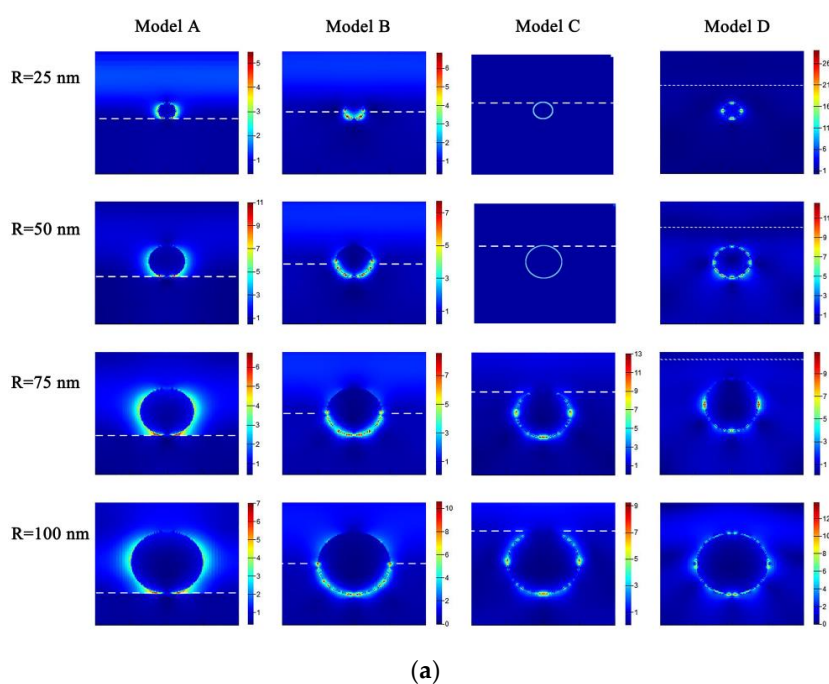


Figure 4. Cont.

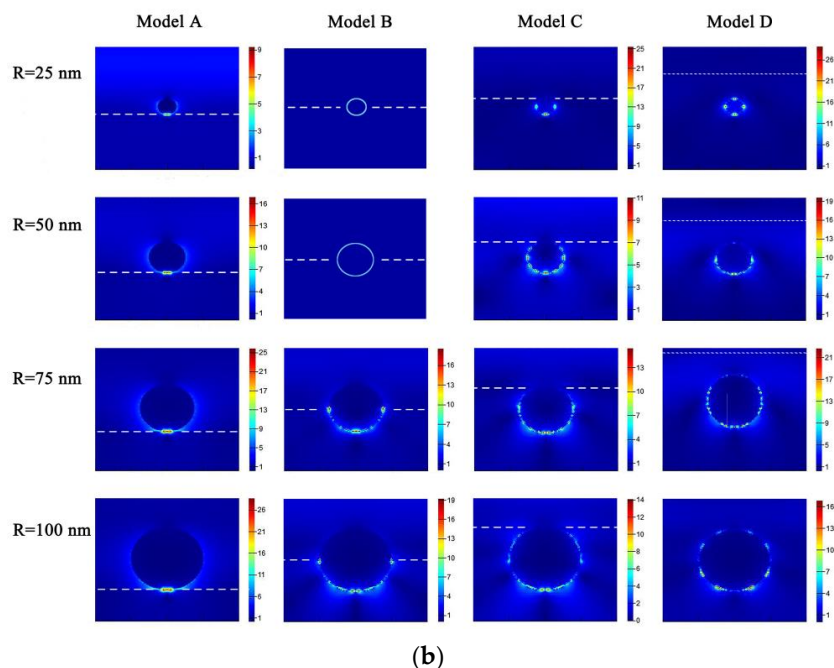


Figure 4. The distribution of the local enhanced electric field of Au nanospheres on a TiO₂ substrate induced by different wavelengths: (a) LSPR absorption peaks; and (b) interband transition peaks. The dashed line represents the interface between the Au nanospheres and the TiO₂ substrate.

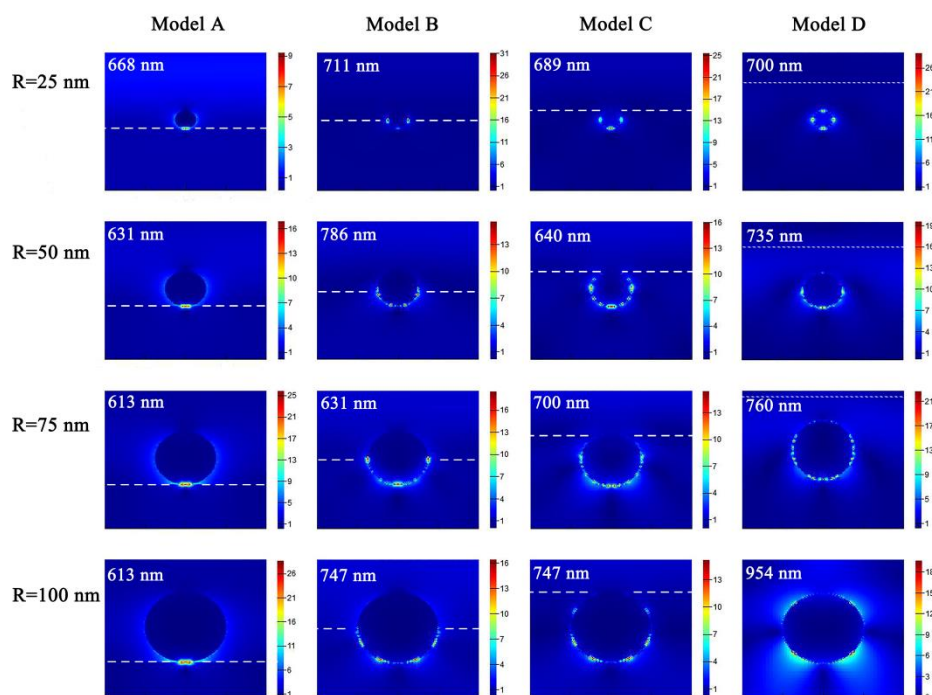


Figure 5. The distribution of the strongest local enhanced electric field of Au nanospheres loaded on the TiO₂ substrate in the whole simulation region of 300–900 nm. The dashed line represents the interface between the Au nanospheres and the TiO₂ substrate.

2.2. Au Nanorods

Compared with Au nanospheres, Au nanorods have different polarization degrees along different directions, due to the structural anisotropy, as shown in Figure 6. If incident light is parallel to the

axial direction of the Au nanorods, the electric field is perpendicular to the axial direction, which induces the lateral resonance ($LSPR_T$). If incident light is perpendicular to the axial direction of the Au nanorods, the electric field is parallel to the axial direction, which induces the longitudinal resonance ($LSPR_L$). In experiments, it is difficult to fix Au nanorods along particular directions. Thus, Au nanorods are usually randomly orientated on the TiO_2 substrate, and produce two distinct resonance absorption peaks. In the theoretical simulation, it is easy to fix Au nanorods along a particular direction. In many experiments, it is a concern that Au nanorods are flattened on the substrate [35,36]. Thus, here we also choose the TiO_2 substrate to be parallel to the axial direction of the Au nanorods. In the present work, the axial direction of the Au nanorods is parallel to the surface of the TiO_2 substrate, in order to study the effects of $LSPR_T$ with respect to different length-diameter ratios (L/D) of Au nanorods with diameters of 100 nm. As shown in Figure 7, for the isolated Au nanorods, when the L/D varies from one to three, the intensity of resonance peak of $LSPR_T$ is increased, while the peak position is almost unchanged (centered at ~ 560 nm), which is consistent with published experimental measurements [13,35,37]. These results suggest that the shape of the Au nanorods is the non-critical factor for the $LSPR_T$ effects.

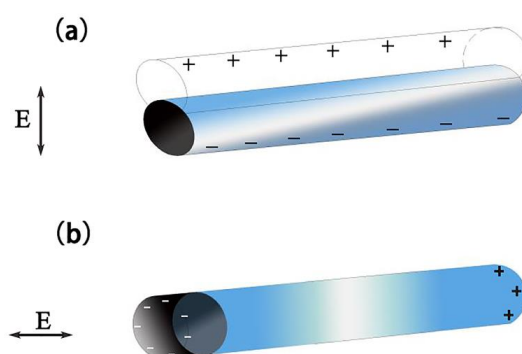


Figure 6. Schematic of two types of LSPR of metallic nanorods: (a) $LSPR_T$; and (b) $LSPR_L$.

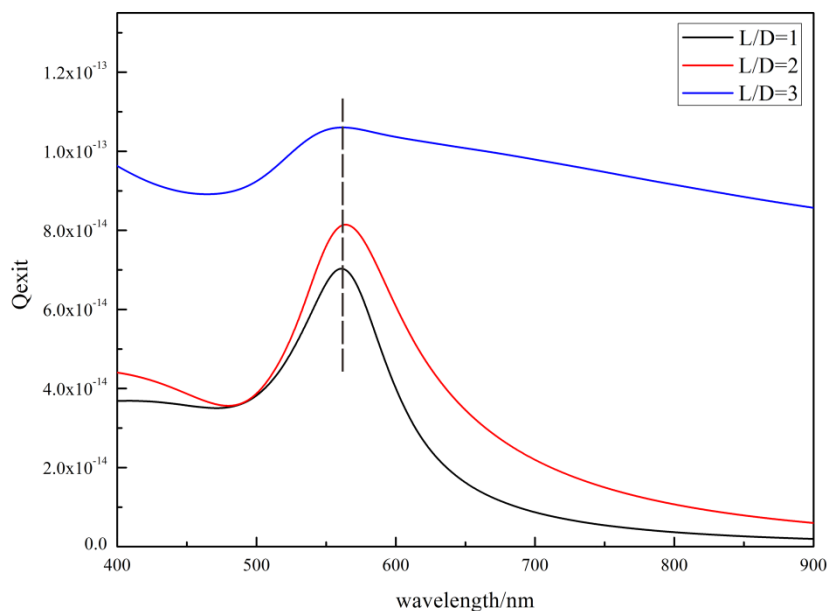


Figure 7. The extinction spectra of isolated Au nanorods with different length-diameter ratios.

The absorption spectra of the Au nanorods with different L/D and locations are plotted in Figure 8. Compared with the clean TiO_2 substrate, as shown in Figure 8a, Au nanorod loading produces some

new absorption bands in the visible-light region. As the ratio of L/D increases, the positions of peaks b, c, and d are red-shifted. On the other hand, the phenomena are very similar with those of Au nanosphere loading. Moreover, these observations are consistent with experimental measurements [35]. When the location of the Au nanorods changes, the absorption properties present some variation. Among these absorption bands, the intensity of the c peak that is induced by the LSPR effect is obviously strong in the case of Au nanorods loaded on the surface of the TiO_2 substrate. As the Au nanorods are gradually embedded into the TiO_2 substrate, the intensity of different absorption bands is, first, gradually decreasing, and then increasing, and the position is gradually red-shifted. These simulated results indicate that the intensity and position of LSPR effects are impacted by the shape and location of Au nanorods.

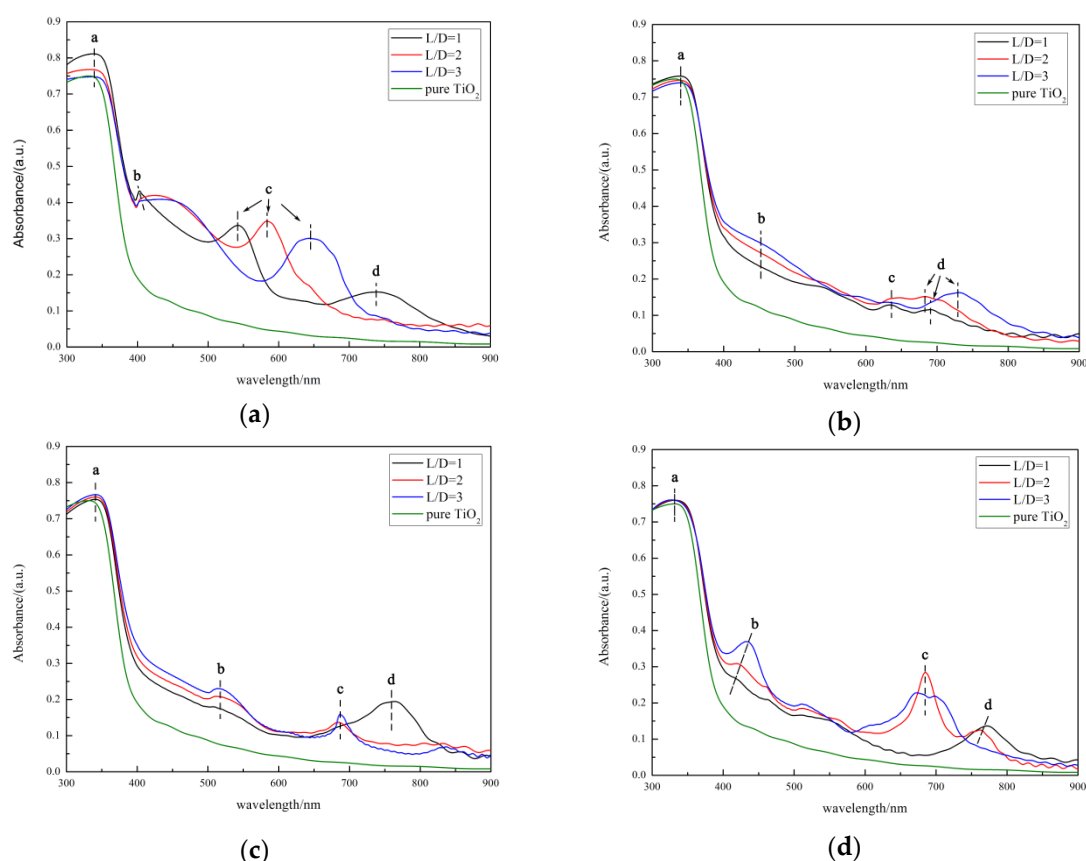


Figure 8. The absorption spectra of Au nanorods loaded on the TiO_2 substrate with different radii and location: (a) Model A, (b) Model B, (c) Model C, and (d) Model D as labeled in Figure 1.

The distribution of the strongest local enhanced electric field in the whole simulation region of 300–900 nm of Au nanorods with different L/D ratios and different locations is illustrated in Figure 9. Similarly, the local enhanced electric fields are presented at the interface between the Au nanorods and the TiO_2 substrate. As the L/D ratio is increasing, the local enhanced electric field is gradually weakening. This phenomenon is very obvious in the case of Au nanorods embedded into the TiO_2 substrate (i.e., Model D). On the other hand, when Au nanorods are gradually embedded into the TiO_2 substrate, the local enhanced electric field is, first, weakening, and then enhancing. This phenomenon is very obvious in the case of Au nanorods with an $L/D = 1$. Moreover, the case of Au nanorods covered by the TiO_2 substrate at 100 nm depths, like the situation of the Au/ TiO_2 core-shell system, can remarkably enhance the local enhanced electric field, and this phenomenon is more obvious with the increase in the thickness of the TiO_2 shell [13,14]. In the photocatalytic activity testing, this effect can significantly promote the photocatalytic performance of TiO_2 .

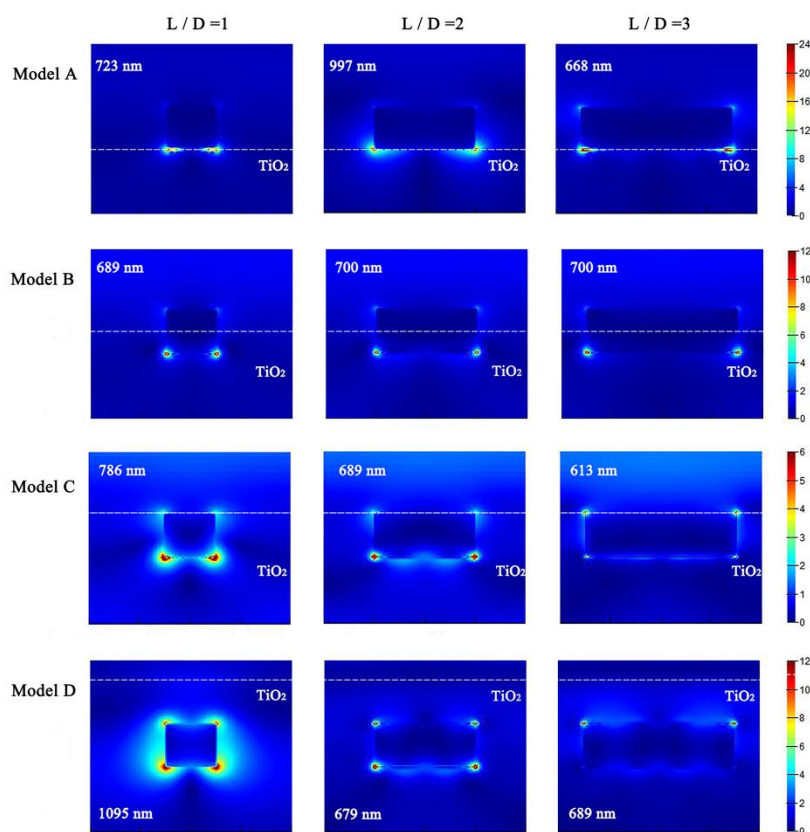


Figure 9. The distribution of the strongest local enhanced electric field of Au nanorods loaded on the TiO₂ substrate in the whole simulation region of 300–900 nm. The dashed line represents the interface between Au nanorods and the TiO₂ substrate.

2.3. Au Nanospheres Versus Au Nanorods Loaded on the TiO₂ Substrate

Due to the different shape and size, the corresponding LSPR of Au nanoparticles present different effects. As the radius of Au nanospheres increases, the LSPR peaks are red-shifted, while as the L/D ratio increases, the LSPR_T peaks remain in almost the same position. When the location of the Au nanoparticles are gradually embedded from the surface to the bulk of the TiO₂ substrate, the LSPR exhibit multi-peak absorption characteristics, especially in the case of Au nanoparticles covered by the TiO₂ substrate (i.e., Model D). In the present work, it is found that adjusting the location of the Au nanoparticles in the TiO₂ substrate could produce more obvious and rich LSPR effects than changing the size of the Au nanoparticles. If the size and location of the Au nanoparticles are fixed, the LSPR effects could appear more significant on the surface of the TiO₂ substrate. In other words, Au nanoparticle loading onto the surface of the TiO₂ photocatalyst may be better to enhance the corresponding performance. Furthermore, the structural anisotropy and complexity of Au nanorods is the root for the non-regular properties of the LSPR effects. For example, Wang et al. have reported that the truncated nanorods exhibit a blue-shift of the LSPR effects in comparison with the rectangular nanorods [22]. It is worth noting that changing the location of the Au nanoparticles in the TiO₂ substrate can vary the LSPR effects, varying from the visible-light region to the near-infrared-light region, while changing the size of the Au nanoparticles only produces about 100-nm red-shifting.

The local enhanced electric fields only present at the interface between the Au nanoparticles and the TiO₂ substrate. When the Au nanoparticles are completely covered by the TiO₂ substrate at a 100-nm depth, the local enhanced electric field is the strongest. In the field of photocatalysis, LSPR can promote the photocatalytic performance (enhance visible-light harvesting, and separate the electron-hole pairs efficiently) by the following effects: direct electron transfer, LSPR-mediated

local electromagnetic fields, and plasmon-induced resonance energy transfer [12,19,32]. However, a recent study suggests that the intensity of the electron transfer is not necessarily correlated with an Au LSPR band [38]. Govorov and co-workers have reported that photo-generated holes in the interband transition are created far from the Fermi surface (2.4 eV relative to E_F), while holes in the plasmonic wave are distributed near the Fermi surface [39]. This means that the 5d band of gold generates a large amount of electrons, and these electrons transition to the conduction band of Au and then to the conduction band of TiO_2 . This promotes efficient separation of electron-hole pairs. In the present work, it can be found that the local enhanced electric fields of the LSPR effect are easily impacted by the shape, size, and location of the Au nanoparticles, compared to the LSPR absorption. Furthermore, there is the complex interaction between the interband transition and LSPR absorption. Thus, how to effectively utilize LSPR effect needs careful consideration to reasonably choose these determined factors according to the enhanced mechanism for the photocatalytic performance.

3. Computational Methods

In recent years, with the aid of computers and various numerical processing methods to solve Maxwell's equations, great achievements have been made in the field of LSPR, such as the FDTD method, discrete dipole approximation (DDA), T-matrix method, discrete source method (DSM), and so on. Among these methods, the FDTD method can directly simulate the near and far field distribution, and can use a non-uniform meshing grid for the irregular models, resulting in relatively high simulation accuracy. The FDTD method is based on the calculation of the Maxwell equations using the Yee cellular discretization shown in Figure 10. It can be seen from Figure 10 that each electric/magnetic field component is surrounded by four magnetic/electric field components. The electric field and the magnetic field are alternately sampled in time. The sampling time interval is half a time step, and solved iteratively in time. Combined with the initial conditions and the boundary conditions, the electromagnetic field distribution in space can be obtained. Through the obtained electric field, the reflectivity, transmissivity, and absorption of incident electromagnetic waves can also be obtained.

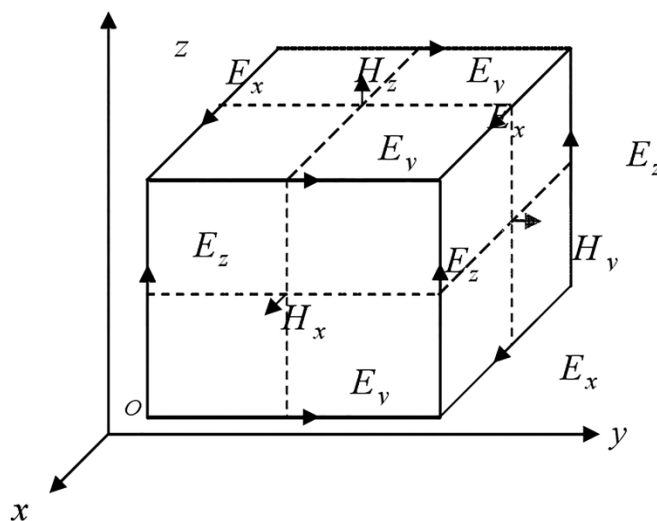


Figure 10. The Yee cells of electromagnetic field in FDTD simulations.

Usually, we used the scattering cross-section (Q_{scat}), the absorption cross-section (Q_{abs}), and the extinction cross-section (Q_{exti}) to characterize the LSPR effects of Au nanoparticles on the TiO_2 substrate. The scattering cross-section characterizes the effective radiation enhancement range of the LSPR, and the absorption cross-section is the effective absorption energy space of the surface electrons for forming the LSPR. While the extinction cross-section is the combined effect of the above two phenomena, which can be used to characterize the integrated effect of the surrounding medium

and metal nanoparticles on the incident electromagnetic field, and observe the effective resonance wavelength between the LSPR and the incident light field. The peak wavelength corresponds to the LSPR wavelength of Au particles. The above physical quantities are related to the size and shape of the gold particles and the surrounding media environment and are defined as follows:

$$Q_{\text{abs}} = k \text{Im}\{\alpha\} = 4ka^3 \text{Im}\left\{\frac{\varepsilon_m - \varepsilon_0}{\varepsilon_m - 2\varepsilon_0}\right\} \quad (1)$$

$$Q_{\text{scat}} = \frac{k^4}{6\pi} |\alpha|^2 = \frac{8}{3} k^4 \pi a^6 \left| \frac{\varepsilon_m - \varepsilon_0}{\varepsilon_m + 2\varepsilon_0} \right|^2 \quad (2)$$

$$Q_{\text{exti}} = Q_{\text{abs}} + Q_{\text{scat}} \quad (3)$$

where k is the wave vector of the incident light, α is the polarizability of the Au nanoparticles, a is the radius of the Au nanoparticles, ε_m and ε_0 are the permittivity of the Au nanoparticles and the environmental medium, respectively, and Im is the imaginary part. In order to simplify the published experimental work [40,41], only one Au nanoparticle in the periodic boundary is considered for the numerical simulation of free electrons' collective oscillation bringing about the LSPR phenomenon in the present work.

In the present work, the dielectric constant of Au can be described using Johnson and Christy's report [42], and the dielectric constant of TiO₂ (anatase) can be introduced using our previous density functional theory calculated results. Other FDTD parameters, descriptions, and settings to extract the optical properties in the present work are listed in Table 2.

Table 2. FDTD parameter descriptions and settings to investigate the optical properties of the proposed Au-based nanoparticles.

Parameter	Isolated Au Nanoparticle	Au/TiO ₂ Composites
Spatial cell sizes(dx = dy = dz)	2.5 nm	2.5 nm
Number of time steps	6000	6000
Source	Total-field scattered-field	Plane wave
Wavelength	300–1500 nm	300–1500 nm
Background index	1	1
Boundary conditions	PML	PML
Number of PML layers	8	12

4. Conclusions

In the present work, the effects of LSPR of Au nanoparticle loading onto a TiO₂ substrate were simulated by the FDTD method. Especially, the variation tendency of the resonance-absorption peaks and the intensity of local enhanced electric field were systematically compared and emphasized. The features of the resonance absorption of LSPR can be tuned by varying the size, shape, and location of Au nanoparticles. When Au nanoparticles are completely embedded into the TiO₂ substrate up to 100-nm, LSPR and interband transition will induce multi-peak absorption characteristics. In these determined factors, the LSPR effects are sensitively dependent on the location of Au nanoparticles in the TiO₂ substrate. When the location of Au nanospheres are gradually immersed into the TiO₂ substrate, the local enhanced electric field of the boundary is gradually enhanced. When it is covered by TiO₂ into 100 nm depths, the local enhanced electric field intensities reach the maximum value. However, when Au nanorods are loaded onto the surface of the TiO₂ substrate, the intensity of the corresponding local enhanced electric field is the maximum. Au nanospheres produce two strong absorption peaks in the visible light region, which are induced by the LSPR effect and interband transitions between Au nanoparticles and the TiO₂ substrate. For the LSPR resonance-absorption peaks, the corresponding position is red-shifted by about 100 nm, as the location of the Au nanospheres is gradually immersed into the TiO₂ substrate. On the other hand, the size change of the Au nanorods does not lead to a

similar variation of the LSPR resonance-absorption peaks, except to change the length-diameter ratio. Meanwhile, the LSPR effects are obviously interfered with by the interband transitions between the Au nanorods and the TiO₂ substrate. In the Au/TiO₂ composite structure, there is a strong interaction between the Au nanoparticles and the TiO₂ substrate, which is compared to the electric field intensity of the Au single-nanoparticle and the composite structure. Furthermore, although interband transitions will interfere with the LSPR, both the interband transitions and the LSPR of Au will have an electric field enhancement effect. Finally, hot electrons are likely to be generated in the 5d band of Au instead of LSPR. The local enhanced electric fields of the LSPR effect are easily impacted by the shape, size, and location of Au nanoparticles, compared to the LSPR absorption. Furthermore, there is the complex interaction between the interband transition and LSPR absorption. Thus, how to effectively utilize the LSPR effect needs careful consideration in order to reasonably choose these determined factors according to the enhanced mechanism of the photocatalytic performance.

Author Contributions: G.-Y.Y. carried out the FDTD calculations, analyzed the calculated results, and prepared the manuscript; Q.-L.L. helped analyze the calculated results and revised the manuscript. Z.-Y.Z. designed and planned the research work, guided G.-Y.Y. to complete the present work, and revised the manuscript.

Acknowledgments: The authors would like to acknowledge the financial support from the National Natural Science Foundation of China (grant no. 21473082), and the 18th Yunnan Province Young Academic and Technical Leaders Reserve Talent Project (grant no. 2015HB015).

Conflicts of Interest: The authors declare no conflict of interest.

References

1. Fujishima, A.; Honda, K. Electrochemical photocatalysis of water at semiconductor electrode. *Nature* **1972**, *238*. [[CrossRef](#)]
2. Xu, M.; Da, P.; Wu, H.; Zhao, D.; Zheng, G. Controlled Sn-doping in TiO₂ nanowire photoanodes with enhanced photoelectrochemical conversion. *Nano Lett.* **2012**, *12*, 1503. [[CrossRef](#)] [[PubMed](#)]
3. Scuderi, V.; Impellizzeri, G.; Romano, L.; Scuderi, M.; Brundo, M.V.; Bergum, K.; Zimbone, M.; Sanz, R.; Buccheri, M.A.; Simone, F.; et al. An enhanced photocatalytic response of nanometric TiO₂ wrapping of Au nanoparticles for eco-friendly water applications. *Nanoscale* **2014**, *6*, 11189–11195. [[CrossRef](#)] [[PubMed](#)]
4. Cao, J.; Zhang, Y.; Tong, H.; Li, P.; Kako, T.; Ye, J. Selective local nitrogen doping in a TiO₂ electrode for enhancing photoelectrochemical water splitting. *Chem. Commun.* **2012**, *48*, 8649–8651. [[CrossRef](#)] [[PubMed](#)]
5. Long, R.; English, N.J. First-principles calculation of synergistic (n, p)-codoping effects on the visible-light photocatalytic activity of anatase TiO₂. *J. Phys. Chem. C* **2010**, *114*, 11984–11990. [[CrossRef](#)]
6. Foo, W.J.; Zhang, C.; Ho, G.W. Non-noble metal Cu-loaded TiO₂ for enhanced photocatalytic H₂ production. *Nanoscale* **2013**, *5*, 759. [[CrossRef](#)] [[PubMed](#)]
7. Liu, L.; Ji, Z.; Zou, W.; Gu, X.; Deng, Y.; Gao, F.; Tang, C.; Dong, L. In situ loading transition metal oxide clusters on TiO₂ nanosheets as co-catalysts for exceptional high photoactivity. *ACS Catal.* **2013**, *3*, 2052–2061. [[CrossRef](#)]
8. Awazu, K.; Fujimaki, M.; Rockstuhl, C.; Tominaga, J.; Murakami, H.; Ohki, Y.; Yoshida, N.; Watanabe, T. A plasmonic photocatalyst consisting of silver nanoparticles embedded in titanium dioxide. *J. Am. Chem. Soc.* **2008**, *130*, 1676–1680. [[CrossRef](#)] [[PubMed](#)]
9. Tanaka, A.; Hashimoto, K.; Kominami, H. A very simple method for the preparation of Au/TiO₂ plasmonic photocatalysts working under irradiation of visible light in the range of 600–700 nm. *Chem. Commun.* **2017**, *53*, 4759–4762. [[CrossRef](#)] [[PubMed](#)]
10. Zhang, S.; Peng, B.; Yang, S.; Wang, H.; Yu, H.; Fang, Y.; Peng, F. Non-noble metal copper nanoparticles-decorated TiO₂ nanotube arrays with plasmon-enhanced photocatalytic hydrogen evolution under visible light. *Int. J. Hydrog. Energy* **2015**, *40*, 303–310. [[CrossRef](#)]
11. Mubeen, S.; Hernandez-Sosa, G.; Moses, D.; Lee, J.; Moskovits, M. Plasmonic photosensitization of a wide band gap semiconductor: Converting plasmons to charge carriers. *Nano Lett.* **2011**, *11*, 5548–5552. [[CrossRef](#)] [[PubMed](#)]

12. Lu, B.; Liu, A.; Wu, H.; Shen, Q.; Zhao, T.; Wang, J. Hollow Au–Cu₂O core–shell nanoparticles with geometry-dependent optical properties as efficient plasmonic photocatalysts under visible light. *Langmuir* **2016**, *32*, 3085–3094. [[CrossRef](#)] [[PubMed](#)]
13. Dai, L.; Song, L.; Huang, Y.; Zhang, L.; Lu, X.; Zhang, J.; Chen, T. Bimetallic Au/Ag core–shell superstructures with tunable surface plasmon resonance in the near-infrared region and high performance surface-enhanced raman scattering. *Langmuir* **2017**, *33*, 5378–5384. [[CrossRef](#)] [[PubMed](#)]
14. Li, Y.; DiStefano, J.G.; Murthy, A.A.; Cain, J.D.; Hanson, E.D.; Li, Q.; Castro, F.C.; Chen, X.; Dravid, V.P. Superior plasmonic photodetectors based on Au@MoS₂ core–shell heterostructures. *ACS Nano* **2017**, *11*, 10321–10329. [[CrossRef](#)] [[PubMed](#)]
15. Ong, W.-J.; Putri, L.K.; Tan, L.-L.; Chai, S.-P.; Yong, S.-T. Heterostructured AgX/g–C₃N₄ (X = Cl and Br) nanocomposites via a sonication-assisted deposition-precipitation approach: Emerging role of halide ions in the synergistic photocatalytic reduction of carbon dioxide. *Appl. Catal. B Environ.* **2016**, *180*, 530–543. [[CrossRef](#)]
16. Chen, L.; Sun, H.; Zhao, Y.; Zhang, Y.; Wang, Y.; Liu, Y.; Zhang, X.; Jiang, Y.; Hua, Z.; Yang, J. Plasmonic-induced sers enhancement of shell-dependent Ag@Cu₂O core–shell nanoparticles. *RSC Adv.* **2017**, *7*, 16553–16560. [[CrossRef](#)]
17. Liu, Y.; Zhou, F.; Zhan, S.; Yang, Y. Preparation of Ag/AgBr–Bi₂MoO₆ plasmonic photocatalyst films with highly enhanced photocatalytic activity. *J. Inorg. Organ. Polym. Mater.* **2017**, *27*, 1365–1375. [[CrossRef](#)]
18. Clarizia, L.; Vitiello, G.; Luciani, G.; Somma, I.D.; Andreozzi, R.; Marotta, R. In situ photodeposited nanoCu on TiO₂ as a catalyst for hydrogen production under UV/visible radiation. *Appl. Catal. A Gener.* **2016**, *518*, 142–149. [[CrossRef](#)]
19. Sugawa, K.; Tsunenari, N.; Takeda, H.; Fujiwara, S.; Akiyama, T.; Honda, J.; Igari, S.; Inoue, W.; Tokuda, K.; Takeshima, N.; et al. Development of plasmonic Cu₂O/Cu composite arrays as visible- and near-infrared-light-driven plasmonic photocatalysts. *Langmuir* **2017**, *33*, 5685–5695. [[CrossRef](#)] [[PubMed](#)]
20. Liu, P.-H.; Wen, M.; Tan, C.-S.; Navlani-García, M.; Kuwahara, Y.; Mori, K.; Yamashita, H.; Chen, L.-J. Surface plasmon resonance enhancement of production of H₂ from ammonia borane solution with tunable Cu_{2–x}S nanowires decorated by Pd nanoparticles. *Nano Energy* **2017**, *31*, 57–63. [[CrossRef](#)]
21. Sun, Y.; Zhao, Z.; Zhang, W.; Gao, C.; Zhang, Y.; Dong, F. Plasmonic bi metal as cocatalyst and photocatalyst: The case of Bi/(BiO)₂CO₃ and Bi particles. *J. Colloid Interface Sci.* **2017**, *485*, 1–10. [[CrossRef](#)] [[PubMed](#)]
22. Wang, H.J.; Yang, K.H.; Hsu, S.C.; Huang, M.H. Photothermal effects from Au–Cu₂O core-shell nanocubes, octahedra, and nanobars with broad near-infrared absorption tunability. *Nanoscale* **2016**, *8*, 965. [[CrossRef](#)] [[PubMed](#)]
23. Zada, A.; Qu, Y.; Ali, S.; Sun, N.; Lu, H.; Yan, R.; Zhang, X.; Jing, L. Improved visible-light activities for degrading pollutants on TiO₂/g–C₃N₄ nanocomposites by decorating SPR Au nanoparticles and 2,4-dichlorophenol decomposition path. *J. Hazard. Mater.* **2017**, *342*, 715–723. [[CrossRef](#)] [[PubMed](#)]
24. Zhu, M.; Cai, X.; Fujitsuka, M.; Zhang, J.; Majima, T. Au/La₂Ti₂O₇ nanostructures sensitized with black phosphorus for plasmon-enhanced photocatalytic hydrogen production in visible and near-infrared light. *Angew. Chem. Int. Ed.* **2017**, *129*, 2096–2100. [[CrossRef](#)]
25. Yoo, S.M.; Rawal, S.B.; Lee, J.E.; Kim, J.; Ryu, H.-Y.; Park, D.-W.; Lee, W.I. Size-dependence of plasmonic Au nanoparticles in photocatalytic behavior of Au/TiO₂ and Au@SiO₂/TiO₂. *Appl. Catal. A Gener.* **2015**, *499*, 47–54. [[CrossRef](#)]
26. Zhu, Y.; Yang, S.; Cai, J.; Meng, M.; Li, X. A facile synthesis of Ag_xAu_{1–x}/TiO₂ photocatalysts with tunable surface plasmon resonance (SPR) frequency used for rhb photodegradation. *Mater. Lett.* **2015**, *154*, 163–166. [[CrossRef](#)]
27. Jiang, Z.Y.; Zhao, Z.Y. Density functional theory study on the metal–support interaction between au₉ cluster and anatase TiO₂ (001) surface. *Phys. Chem. Chem. Phys.* **2017**, *118*, 3514–3522. [[CrossRef](#)] [[PubMed](#)]
28. Rao, C.N.R.; Kulkarni, G.U.; Thomas, P.J.; Edwards, P.P. Size-dependent chemistry: Properties of nanocrystals. *Chem. A Eur. J.* **2002**, *8*, 28–35. [[CrossRef](#)]
29. Winsemius, P.; Guerrisi, M.; Rosei, R. Splitting of the interband absorption edge in Au: Temperature dependence. *Phys. Rev. B* **1975**, *12*, 4570–4572. [[CrossRef](#)]
30. Liu, L.; Li, P.; Adisak, B.; Ouyang, S.; Umezawa, N.; Ye, J.; Kodyath, R.; Tanabe, T.; Ramesh, G.V.; Ueda, S. Gold photosensitized SrTiO₃ for visible-light water oxidation induced by Au interband transitions. *J. Mater. Chem. A* **2014**, *2*, 9875–9882. [[CrossRef](#)]

31. Pakizeh, T. Optical absorption of plasmonic nanoparticles in presence of a local interband transition. *J. Phys. Chem. C* **2011**, *115*, 21826–21831. [[CrossRef](#)]
32. Li, J.; Cushing, S.K.; Bright, J.; Meng, F.; Senty, T.R.; Zheng, P.; Bristow, A.D.; Wu, N. Ag@Cu₂O core-shell nanoparticles as visible-light plasmonic photocatalysts. *ACS Catal.* **2014**, *3*, 47–51. [[CrossRef](#)]
33. Sönnichsen, C.; Franzl, T.; Wilk, T.; von Plessen, G.; Feldmann, J.; Wilson, O.; Mulvaney, P. Drastic reduction of plasmon damping in gold nanorods. *Phys. Rev. Lett.* **2002**, *88*, 077402. [[CrossRef](#)] [[PubMed](#)]
34. Jin, R. Quantum sized, thiolate-protected gold nanoclusters. *Nanoscale* **2010**, *2*, 343–362. [[CrossRef](#)] [[PubMed](#)]
35. Hu, C.; Rong, J.; Cui, J.; Yang, Y.; Yang, L.; Wang, Y.; Liu, Y. Fabrication of a graphene oxide–gold nanorod hybrid material by electrostatic self-assembly for surface-enhanced raman scattering. *Carbon* **2013**, *51*, 255–264. [[CrossRef](#)]
36. Wang, Z.; Cao, M.; Yang, L.; Liu, D.; Wei, D. Hemin/Cu nanorods/self-doped TiO₂ nanowires as a novel photoelectrochemical bioanalysis platform. *Analyst* **2017**, *142*, 2805–2811. [[CrossRef](#)] [[PubMed](#)]
37. Oyelere, A.K.; Chen, P.C.; Huang, X.; El-Sayed, I.H.; El-Sayed, M.A. Peptide-conjugated gold nanorods for nuclear targeting. *Bioconjug. Chem.* **2007**, *18*, 1490. [[CrossRef](#)] [[PubMed](#)]
38. Priebe, J.B.; Michael, K.; Henrik, J.; Matthias, B.; Dirk, H.; Angelika, B. Water reduction with visible light: Synergy between optical transitions and electron transfer in Au–TiO₂ catalysts visualized by in situ EPR spectroscopy. *Angew. Chem. Int. Ed.* **2013**, *52*, 11420–11424. [[CrossRef](#)] [[PubMed](#)]
39. Govorov, A.O.; Zhang, H.; Gun'ko, Y.K. Theory of photoinjection of hot plasmonic carriers from metal nanostructures into semiconductors and surface molecules. *J. Phys. Chem. C* **2013**, *117*, 16616–16631. [[CrossRef](#)]
40. Liu, S.; Chen, G.; Prasad, P.N.; Swihart, M.T. Synthesis of monodisperse Au, Ag, and Au–Ag alloy nanoparticles with tunable size and surface plasmon resonance frequency. *Chem. Mater.* **2011**, *23*, 4098–4101. [[CrossRef](#)]
41. Kimura, K.; Naya, S.I.; Jin-Nouchi, Y.; Tada, H. TiO₂ crystal form-dependence of the au/TiO₂ plasmon photocatalyst's activity. *J. Phys. Chem. C* **2012**, *116*, 7111–7117. [[CrossRef](#)]
42. Johnson, P.B.; Christy, R.W. Optical constants of the noble metals. *Phys. Rev. B* **1972**, *6*, 4370–4379. [[CrossRef](#)]



© 2018 by the authors. Licensee MDPI, Basel, Switzerland. This article is an open access article distributed under the terms and conditions of the Creative Commons Attribution (CC BY) license (<http://creativecommons.org/licenses/by/4.0/>).